Accepted Manuscript

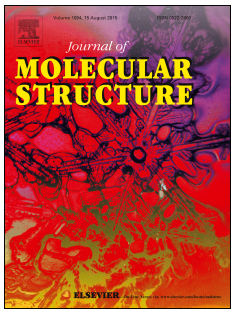

Synthesis, spectral characterization, quantum chemical calculations, in-vitro antimicrobial and DNA activity studies of 2-(2′-mercaptophenyl) benzothiazole complexes

Reda A. Ammar, Amani S. Alturiqi, Abdel-Nasser Alaghaz, Mohamed E. Zayed

PII: S0022-2860(18)30609-4

DOI: 10.1016/j.molstruc.2018.05.043

Reference: MOLSTR 25216

To appear in: *Journal of Molecular Structure*

Received Date: 6 December 2017

Revised Date: 16 April 2018

Accepted Date: 11 May 2018

Please cite this article as: R.A. Ammar, A.S. Alturiqi, A.-N. Alaghaz, M.E. Zayed, Synthesis, spectral characterization, quantum chemical calculations, in-vitro antimicrobial and DNA activity studies of 2-(2′-mercaptophenyl) benzothiazole complexes, *Journal of Molecular Structure* (2018), doi: 10.1016/j.molstruc.2018.05.043.

Revised Manuscript

Synthesis, spectral characterization, Quantum Chemical calculations, *in-vitro* antimicrobial and DNA activity studies of 2-(2'-mercaptophenyl) benzothiazole complexes

Reda A. Ammar [a], Amani S. Alturiqi [b], Abdel-Nasser M.A. Alaghaz [c,d] and Mohamed E. Zayed[e]

[a] Department of Chemistry, College of Science, Al-Imam Mohammad Ibn Saud Islamic University (IMSIU), 13623 Riyadh, Saudi Arabia.
[b] Department of Chemistry, College of Science, Princess Nourah bint Abdul Rahman University, Saudi Arabia.
[c] Department of Chemistry, Faculty of Science, Jazan University, Jazan, Saudi Arabia.
[d] Department of Chemistry, Faculty of Science (Boys), Al-Azhar University, Cairo, Egypt.
[e] Department of Botany and Microbiology, Faculty of Science, King Saud University, Riyadh 11541, Saudi Arabia

Abstract

New ligand (HMPBT) ligand is prepared via condensation of 2-mercaptoaniline and 2-mercaptobenzoic acid in 1:1 ratio. Metal complexes are prepared and characterized by different physical techniques (IR, UV/Vis., ^{1}H NMR, ^{13}CNMR, TGA, DTA, DSC, XRD, magnetic moment and electrical conductance measurements). From the elemental analyses data, the complexes were proposed to have the general formulae [M(MPBT)$_2$] (where M= Co(II), Ni(II), Cu(II) and Zn(II) and MPBT = Ligand. The molar conductance data reveal that all the metal chelates were non-electrolytes. Infrared spectra of the complexes indicate deprotonation and coordination of the thiol –SH. It also confirms that nitrogen atom of the benzothiazole group contribute to the complexation. Electronic spectra and magnetic susceptibility measurements as well as quantum chemical calculations reveal square planar geometry for Cu(II) and Ni(II) complexes and tetrahedral geometry for Co(II) and Zn(II) complexes. The activation of thermodynamic parameters are calculated using Coast-Redfern (CR), Horowitz–Metzger (HM), and Piloyan–Novikova (PN). The geometries of the complexes are confirmed using DFT method from DMOL^3 calculations and ligand field parameters. The investigated ligand and metal complexes were screened for their *in-vitro* antimicrobial activities against different types of fungal and bacterial strains. The resulting data assert on the inspected compounds as a highly promising bactericides and fungicides. The binding activities of zinc (II) complex with CT-DNA was investigated using absorption titration, fluorescence spectroscopy and cyclic voltammetry measurements in a Tris-HCl buffer system at pH 7.0. In addition to these methods, gel electrophoresis and viscosity measurements were also carried out to determine DNA-binding activities with zinc (II) complex in a buffer

solution. The results indicated that zinc (II) complex interacts strongly with CT-DNA through the intercalative binding mode.

Keywords: Complexes; Spectroscopic; Thermal; DFT calculations; Biological activity

Email address:aalajhaz@hotmail.com (Abdel-Nasser M. A. Alaghaz)

1. Introduction

Compounds containing sulfur are omnipresent in nature. These compounds include thiophosphate pesticides, antibacterial agents (e.g., penicillins and cephalosporins), and important biological agents and metabolites (e.g., cysteine, homocysteine, glutathione, coenzyme A, and biotin). Sulfhydryl groups –SH are the most reactive in protein molecules (enzymatic and receptor), and the possibility of their chemical modification has an important regulative role [1–3]. Furthermore, sulfur-containing organic compounds and especially aromatic thiols have attracted enormous attention due to theirs potential applications in molecular electronic devices, taking advantage of their high conductivity and nonlinear optical properties [4]. Due to the importance and useful properties of Sulfur-containing compounds, the scope and application of these compounds have increased tremendously [5]. On the other hand, many chemical processes in these systems are modulated by the existence or the formation of intramolecular hydrogen bonds (HBs). The 2-(*E*)-imino methyl benzenethiol (IBT) is one of the interesting benzenethiol derivatives, which involved in the S–H···N intramolecular hydrogen bonding. HB in its various aspects continues to be a topic of extreme scrutiny in various chemical and biological systems, as it plays a vital role in stabilizing molecular structures, and modulating specificity and speed of enzymatic reactions [6–8]. The hydrogen bonds can effect on the molecular structure and properties in the excited state. On the other hand, time-dependent DFT (TD-DFT) method has been demonstrated as an effective way to theoretically study HBs in different electronic states [9–11]. In the present work, 2-(2'-mercaptophenyl)benzothiazole and their corresponding metal complexes have been studied. The geometry of the complexes is characterized by means of spectral, magnetic, thermal studies and DFT calculations. Also, the biological activities of the ligand and their metal complexes have been investigated.

2. Experimental

2.1. Materials and methods

The 2-mercaptoaniline and 2-mercaptobenzoic acid molecules used in this study were obtained from commercial source (Sigma-Aldrich) and were used without any purification. Elemental analyses (C, H, N, S) were performed on a Perkin–Elmer 2408 CHN Analyzer. Molar conductivities were measured in DMSO solution of the complexes (10^{-3} M) using a CON 6000 conductivity meter, Cyberscan, Eutech instruments. The FT-IR spectra were recorded at the interval 400–4000 cm^{-1} at room temperature on a Perkin-Elmer Spectrum Two FT-IR Spectrometer with 0.5 cm^{-1} standard resolution in the transmission mode in solid phase of sample. The sample were compressed into self-supporting pellet and introduced into an IR cell equipped with KBr window. The ^{1}H and ^{13}C NMR chemical shift experiments were performed with BRUKER BIOSPIN-AVANCE III 400 MHz NMR spectrometer at temperature of 295 K. The samples were dissolve in DMSO. The chemical shifts were reported at ppmlevel relative to tetramethylsilane (TMS). The ^{1}H and ^{13}C NMR chemical shift values were obtained at a frequency of 400 MHz. The mass spectra were recorded by the EI technique at 70 eV using MS-5988 GC–MS Hewlett–Packard instrument in the Microanalytical Center, Cairo University. Magnetic susceptibilities of the complexes were measured by the modified Gouy method at room temperature using Magnetic Susceptibility Johnson Matthey Balance. The effective magnetic moments were calculated using the relation $\mu_{eff} = 2.828(\chi_m T)^{1/2}$ B.M., where χ_m is the molar magnetic susceptibility corrected for diamagnetism of all atoms in the compounds using Selwood and Pascal's constants. Electronic spectra were recorded on a UV2 Unicam UV/Vis Spectrophotometer. EPR spectra of Co(II), Ni(II) and Cu(II) the complexes were recorded as polycrystalline samples, at room temperature, on an E4-EPR spectrometer using the DPPH as the *g*-marker. The X-ray diffraction patterns for the obtained metal(II) complexes were collected on a PANalytical X'Pert PRO X-ray powder diffractometer at the Central Lab at Ain Shams University, Egypt. The instrument was equipped with a Ge (III) monochromator, and a Cu $K\alpha_1$ X-ray source with a wavelength of 0.154056 nm was used. Thermal analysis (TG/DTG) were obtained out by using a Shimadzu DTA/TG-50 Thermal analyzer with a heating rate of 10 °C /min in nitrogen atmosphere with a following rate 20 mL/min in the temperature range 30–600 °C using platinum crucibles. Melting points obtained with a Yanagimoto micro-melting point apparatus are uncorrected. The biological activity experiments were carried out at the Microbiology Laboratory at Bab-Al-Sheria Hospital, Al-Azhar University.

2.2. Synthesis of the ligand (HMPBT)

Hot solution (60 °C) of 2-mercaptoaniline (2.50 g, 20 mmol) was mixed with hot solution (60 °C) of 2-mercaptobenzoic acid (3.08 g, 20 mmol) in 50 ml ethanol. The resulting mixture was left under reflux for 3 h and the solvent was evaporated till deep yellow oil product is separated. This oil is poured on ice cold dilute HCl whereupon the yellow crystalline product is separated. The formed solid product was separated by filtration,

purified by crystallization from ethanol, washed with diethyl ether and dried in a vacuum over anhydrous calcium chloride. The yellow product is produced in 88% yield.

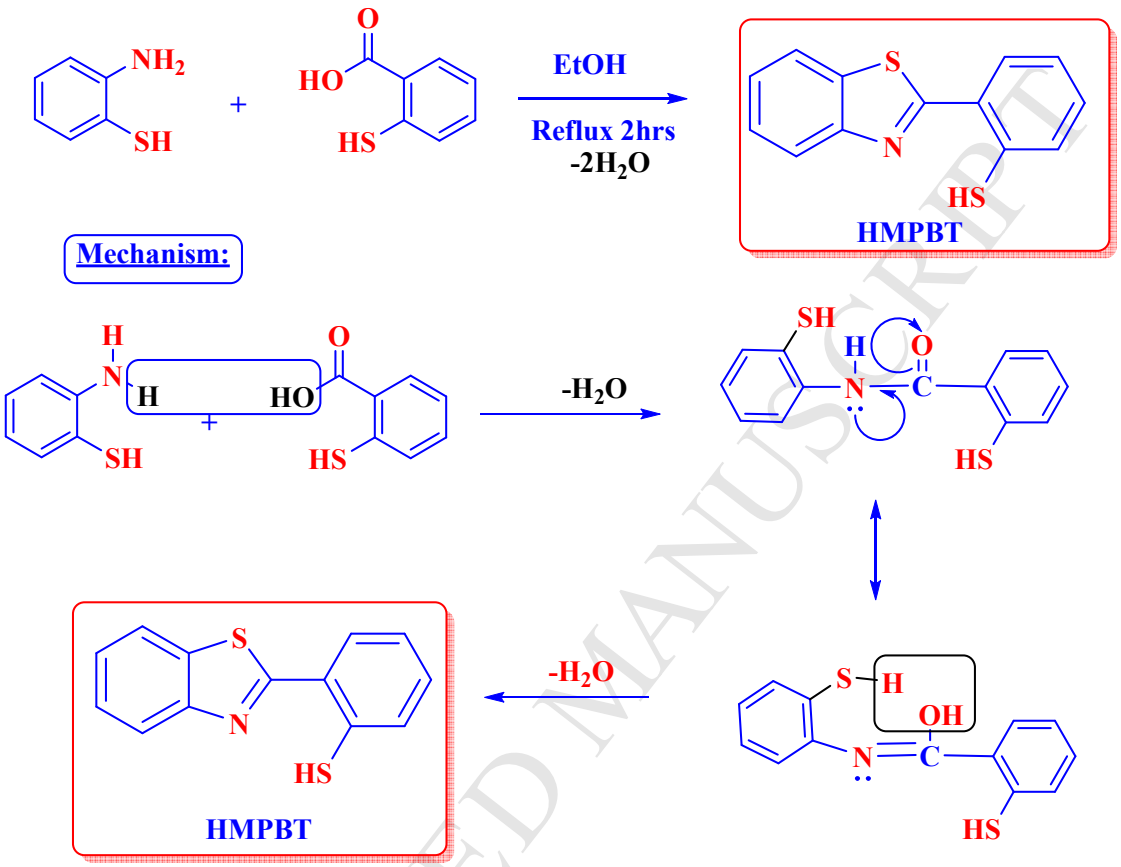

Scheme 1. Synthesis and mechanism of the prepared ligand (HMPTB).

2.3. Synthesis of the metal complexes (1-4)

The metal complexes were prepared by the addition of hot solution (60 °C) of the appropriate metal chloride or sulfate (1 mmol; $CoCl_2.6H_2O$: 0.238 g, $NiCl_2.6H_2O$: 0.238 g, $CuCl_2.2H_2O$: 0.171 g, $ZnSO_4.7H_2O$: 0.288 m) in an ethanol–water mixture (1:1, 25 ml) to the hot solution (60 °C) of the ligand HMPBT (2 mmol; 0.487 g) in the same solvent (25 ml). The resulting mixture was stirred under reflux for one hour whereupon the complexes precipitated. They were collected by filtration, washed with a 1:1 ethanol: water mixture and diethylether and dried in vacuum over anhydrous $CaCl_2$.

2.4. Quantum chemical calculations

The calculations using DMOL3 program were performed in Materials Studio package [13], which is designed for the realization of large scale density functional theory (DFT) calculations. DFT semi–core pseudo pods calculations (dspp) were performed with the

double numerical basis sets plus polarization functional (DNP). The DNP basis sets are of comparable quality to 6–31G Gaussian basis sets [14]. Delley et al. showed that the DNP basis sets are more accurate than Gaussian basis sets of the same size [15]. The RPBE functional [16] is so far the best exchange–correlation functional [17], based on the generalized gradient approximation (GGA), is employed to take account of the exchange and correlation effects of electrons. The geometric optimization is performed without any symmetry restriction.

2.5. Antimicrobial investigation

Antimicrobial Activity

The *in vitro* biological screening effects of the ligand and its complexes were tested against the bacterial species *E. coli* and *S. aureus*, fungal species *P. aeriginosa* and *B. subtilis* by the cup plate method at 1 mg/mL concentration.

The bacterial and fungal cultures were inoculated in nutrient broth (inoculation medium) and incubated overnight at 37°C. Inoculated medium containing 24 h grown culture was added aseptically to the nutrient medium and mixed thoroughly to get a uniform distribution. This solution was poured (25 mL in each dish) into Petri dishes and then allowed to attain room temperature. Wells (6 mm in diameter) were punched carefully using a sterile cork borer and were filled with test solution 25 μL. The plates were allowed to stand for an hour in order to facilitate the diffusion of the drug solutions, then the plates were incubated at 37°C for 24 h for bacteria and 48 h for fungi and the diameter of the zone of inhibition was measured [18]. The results were compared with those of standard drug streptomycin for bacterial and captan for fungal activity of the same concentration as that of the test compounds under identical conditions.

2.6. DNA binding

2.6.1. Absorption and Fluorescence Spectroscopy Studies

Absorption titrations for DNA-binding experiments were performed at room temperature at pH 7.0 in a 20 mM Tris-HCl buffer system containing 20 mM of NaCl. The concentration of Calf Thymus (CT)-DNA was calculated by UV/Vis absorbance at 255 nm by using a DNA molar extinction constant (ε) of 6600 $M^{-1}cm^{-1}$, indicating that the DNA solution was protein free [19]. Absorption spectra measurements were conducted in the region of 300 to 800 nm. Absorption titrations for Zinc(II) complex at

fixed concentrations of the Zinc(II) complex in a Tris-HCl buffer solution at pH 7.0 were carried out by adding from 0 to 3 µM of CT-DNA. In order to determine the dilution effects, they were compared to control titrations with a buffer system instead of CT-DNA [20].

Fluorescence spectra were carried out in the region of 540 to 770 nm after excitation at 640 nm. Titration of Zinc(II) complex with CT-DNA was conducted by adding a small amount of a concentrated CT-DNA solution to the Zinc(II) complex solution at a fixed concentration. The solutions were permitted to reach equilibrium for 5 minutes before measurements were recorded [21].

2.6.2. Cyclic Voltammetry Studies

Cyclic voltammetry studies at the glassy carbon electrode used an Ivisumstat Electrochemical Interface electrochemical analyzer at the following settings: Initial potential was −1.5 V and the final potential was 1.5 V; the scan rate was 10 mV/s. A glassy carbon working electrode, an Ag/AgCl reference electrode and a platinum wire counter electrode were used in this study. A standard single compartment three electrode cell system of 10 mL capacity was used to carried out all the measurements [22]. All cyclic voltammetry measurements were recorded at room temperature in a Tris-HCl buffer at pH 7.0.

2.6.3. DNA cleavage

For the DNA cleavage study, the CT-DNA in 20 mM of Tris-HCl buffer system at pH 7.0 containing 20 m M NaCl was used to interact with Zinc(II) complex. The interaction of Zinc(II) complex with CT-DNA was investigated using a 1% agarose gel in Tris-HCl buffer EDTA (TBE). Samples of 20 µL of CT-DNA plus Zinc(II) complex were loaded with dye. The agarose gel electrophoresis experiment was carried out at 80 V for 3 hours in Tris buffer EDTA (TBE). After the gel electrophoresis experiment, CT-DNA bands were visualized by using a Vilber Lourmat UV lamp. For this experiment, the Thermo Scientific Owl gel electrophoresis system was used.

3. Results and discussion

The analytical data (Table 1) agree well with the formula of the ligand and their complexes. The isolated complexes are soluble in ethanol, methanol, DMF and DMSO but insoluble in most other organic solvents. The molar conductance values (Table 1) of 10^{-3}M solutions lie in the range of 7.79-10.26 $\Omega^{-1}cm^2mol^{-1}$ in dry DMSO indicating their non-electrolytic nature. Thus, the complexes may be formulated as $[M(MPBT)_2]$, where M= Co(II), Ni(II), Cu(II) and Zn(II), MPBT = ligand.

Table 1
Physical and elemental analysis data of the ligand HMPBT and its metal (II) complexes

Cpd.	M.F.(M.Wt.)	M.p.(°C)	Colour [Yield %]	Elemental analyses Found (Calc.), %					[a]Λ_m
				C	H	N	S	M	
Ligand	HMPBT	134-1136	Orange	64.17	3.73	5.76	26.35	–	–
	$C_{13}H_9NS_2$ (243.3)		[88]	(64.17)	(3.73)	(5.76)	(26.35)		
1	$[Co(MPBT)_2]$	182	Faint brown	57.45	2.97	5.15	23.59	10.84	9.57
	$C_{26}H_{16}N_2S_4Co$(543.6)		[82]	(57.45)	(2.97)	(5.15)	(23.59)	(10.84)	
2	$[Ni(MPBT)_2]$	190	Dark brown	57.47	2.97	5.16	23.60	10.80	8.36
	$C_{26}H_{16}N_2S_4Ni$ (543.4)		[83]	(57.47)	(2.97)	(5.16)	(23.60)	(10.80)	
3	$[Cu(MPBT)_2]$	182	Reddish brown	56.96	2.94	5.11	23.39	11.59	7.79
	$C_{26}H_{16}N_2S_4Cu$ (548.2)		[87]	(56.96)	2.94)	(5.11)	(23.39)	(11.59)	
4	$[Zn(MPBT)_2]$	180	Orange	56.77	2.93	5.09	23.31	11.89	7.87
	$C_{26}H_{16}N_2S_4Zn$ (550.0)		[74]	(56.77)	(2.93)	(5.09)	(23.31)	(11.89)	

3.1. Quantum chemical calculations of (HL) and its metal complexes

Since single crystal x-ray structure for the ligand is not available, quantum chemical calculations were utilized to find the geometry optimized structures for the HMPBT at different quantum mechanical levels. The molecular modeling is the blue print of three dimensional arrangements of atoms of any compounds. A Higher value of E_{HOMO} is likely to indicate a tendency of the molecule to donate electrons to appropriate acceptor molecule of low empty molecular orbital energy [23]. Increasing values of E_{HOMO} facilitate adsorption and therefore enhance the inhibition efficiency, by influencing the transport process through the adsorbed layer [24]. Total energy represents the importance gaudiness of the ease of chemical reaction; it means the sum of kinetic and potential energy [25]. The negative total energy also indicates that the product is a very stable molecule and is less prone to be split or broken [26]. The governing principle of DFT involves solving the Schrödinger equation in terms of the electron density [27]. DFT is also able to describe site selectivity or reactivity of an atom in a molecule [28].

If deviations in bond distance, bond angles or torsion angles are evidenced, specific electronic interactions can be detected and confirmed to the earlier spectral evidences [29]. Thus, physical dimension of the molecules helped out to demonstrate the changes occurred during their topological assemblies.

The molecular structures along with atom numbering, electron density, hydrogen bond length, hydrogen bond angle, HOMO, LUMO and electrostatic potential of the ligand (HMPBT) are depicted in Figure 1, where the same characters are represented for the metal complexes by the Figures 2, 1S - 3S.

Comparison between the bond lengths and bond angles of the ligand and the Co(II), Ni(II), Cu(II) and Zn(II) complexes are listed in the Tables S1, S2, respectively. Various energetic data were calculated and reported (Table S3).

According to these data a lot of conclusions are revealed:

- The actual bond angles and lengths are close to the optimal values, and thus the proposed structures of the compounds are acceptable.

- The values 1.876 Å and 142.296^{o} are the hydrogen bond length N(7)-H(25) and its bond angle N(7)-H(25)-S(16) which disappear upon coordination as the ligand is deprotonated.
- As expected, the bonds C(4)-N(7) and C(11)-S(16) affected on complexation as they contribute in the coordination sphere where, C(5)-S(9) shows no change.
- Depending on the values of bond lengths the Ni-N(7) < Ni-N(23) < Co-N(7) = Co-N(23) < Cu-N(23) < Cu-N(7) and Zn-N(7) < Zn-N(23) the comes the M-S bonds and arranged as the Ni-S(16) < Ni-S(32) < Co-S(16) = Co-S(32) < Cu-S(16) < Cu-S(32) and Zn-S(32) < Zn-S(16) implies that the Ni^{II}- N(7) is the most stable bond where the least stable bond is that formed by Zn^{II}-S(16).
- The bond angles C(4)-N(7)-C(8), C(10)-C(11)-S(16), C(20)-N(23)-C(24) and C(26)-C(27)-S(32) of the ligand are reduced or increased upon coordinaion [30].
- New bond angles were formed between the ligand and metal ions as N(7)-M(33)-S(16), N(7)-M(33)-N(23), N(7)-M(33)-S(32), S(16)-M(33)-N(23), S(16)-M(33)-S(32) and N(23)-M(33)-S(32) with different values ranges between (90.052^{o}-151.719^{o}) [31].
- Electrostatic potentials provide information about electron-poor and electron-rich sites in a molecule, and electrostatic interactions between molecules [32], therefore the structure of the electrostatic potential of the ligand and complexes was important to be depicted.
- The higher HOMO energy lies around the hetero-ring neglecting the phenyl group while the lower LUMO energy involves both of them.

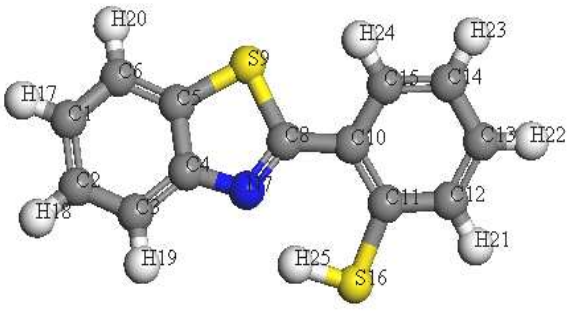

Molecular structure

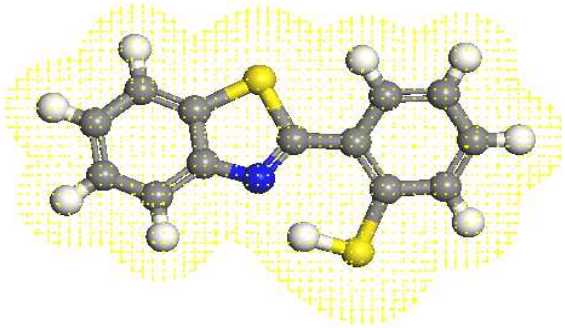

Electron density

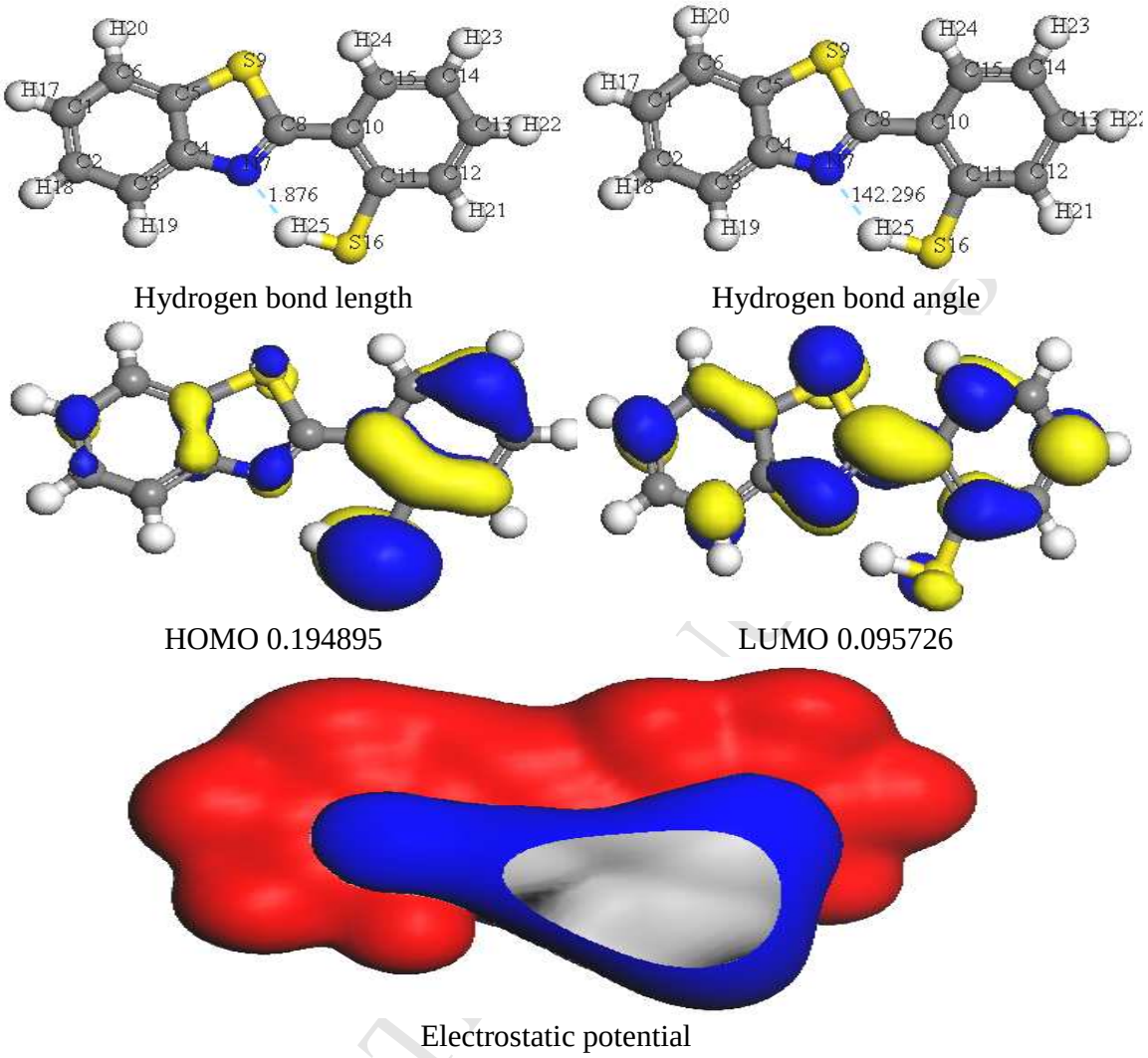

Hydrogen bond length Hydrogen bond angle

HOMO 0.194895 LUMO 0.095726

Electrostatic potential

Figure 1. The molecular structure, electron density, hydrogen bond length, hydrogen bond angle, HOMO, LUMO and electrostatic potential of the ligand (HMPBT).

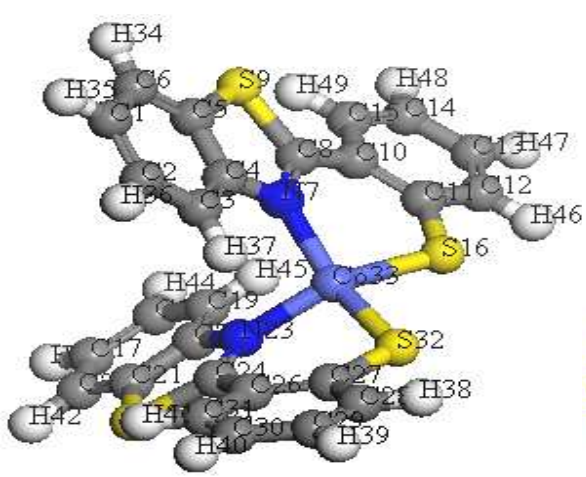

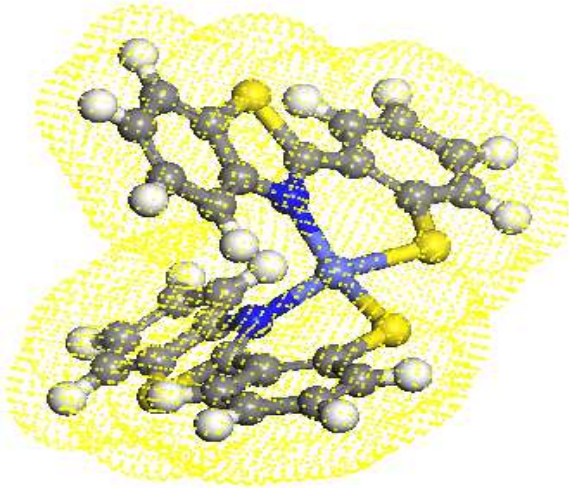

Molecular structure Electron density

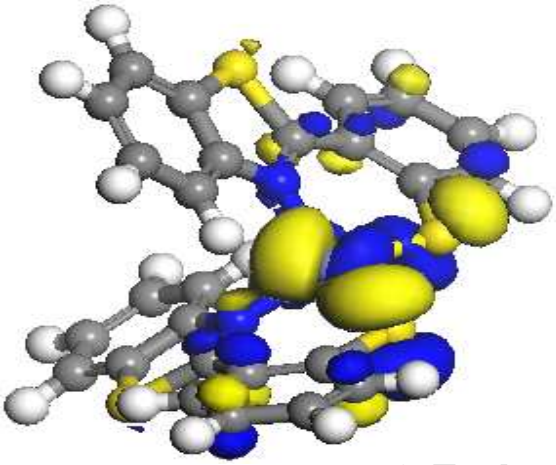

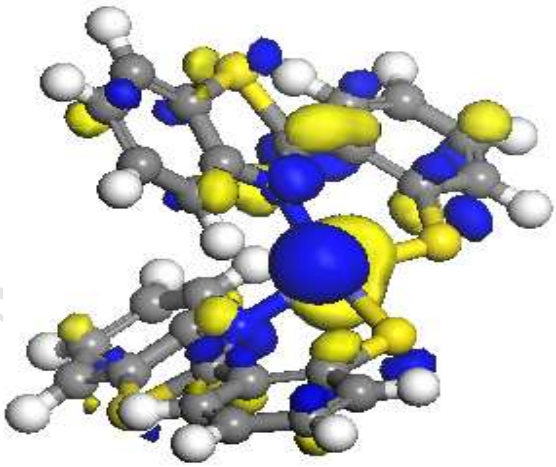

HOMO 0.15502 LUMO 0.105865

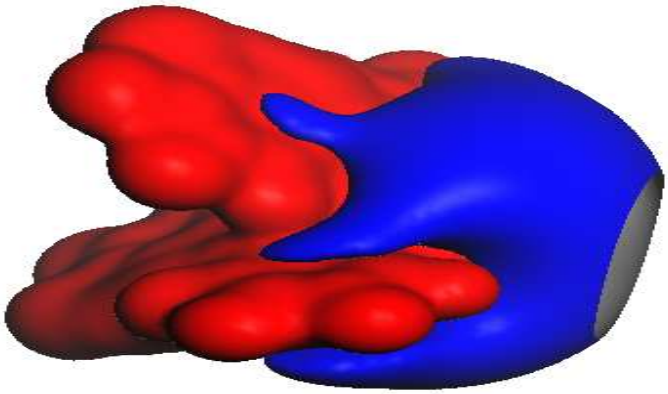

Electrostatic potential

Figure 2. The molecular structure, electron density, HOMO, LUMO and electrostatic potential of $[Co(MPBT)_2]$ complex.

3.2. IR spectra and mode of bonding

In order to characterize the binding mode of the Schiff base to the metal ion in the complexes, the IR spectrum of the free ligand was compared with the spectra of the metal complexes. The IR spectra of the free ligand and metal complexes were carried out in the range 4000–400 cm^{-1} (Figure S4, Table 2). The band centered at about 2652 cm^{-1} are assigned to ν(S–H) in S–H---N intramolecular (Figure 3) hydrogen-bonding fragment [33]. Very strong band centered at 1119 cm^{-1} is assigned to ν(C=S) stretching in HMPTB ligand [33]. The deprotonation of the thiol group (S–H) is indicated by the absence of a band in the metal complexes at 2652 cm^{-1}, which appears due to ν(S–H) in the spectrum of the ligand indicating thereby complexation through sulfur atom. The free ligand shows a sharp intense band at 1623 cm^{-1}assigned to the *ν* (C = N) of the benzothiazole ring [34, 35]. The *ν* (C = N) benzothiazole vibration of the ligand is shifted to 1602–1606 cm^{-1} after complexation, confirming the formation of a bond from the benzothiazole ring nitrogen to the metal. Further, the non-ligand bands in the region 504–523 cm^{-1} and 426–437 cm^{-1} are due to the formation of M-N and M-S bonds, respectively [34, 35]. Noninvolvement of sulfur of the benzothiazole in coordination is assumed in all these complexes, which is in accordance with earlier reports [36] on the benzothiazole complexes with various transition metal ions, this is because the sulfur is a poor Lewis base compared to nitrogen in the benzothiazole [37]. For the title compounds, CH stretching vibrations of the phenyl rings are assigned in the range 3105–3084 $cm^{-1}$for. The phenyl CH stretching modes are observed at 3084 to 3058 cm^{-1}. The in-plane CH deformation bands of the phenyl ring are expected above 1000 cm^{-1} and in the present case, the bands at 1283, 1174, 1154, 1104, 1092, 1058 cm^{-1}. The CH out-of-plane deformations of the phenyl ring are observed between 1006 and 703 cm^{-1}. In conclusion, these data suggest a NS bidentate behavior of the ligand.

Table 2
Important IR bands of HMPBT ligand and its complexes with their assignments.

Compounds	assignments				
	ν(S–H)	ν(–C=N–)	ν(–C=S)	ν(M–N)	ν(M–S)
HMPBT	2652(br)	1623m	1119	–	–
[Co(HMPBT)$_2$]	–	1603m	1313m,	512m	426m
[Ni(HMPBT)$_2$]	–	1602m	1266m	504m	432m
			1322m,		
			1268m		
[Cu(HMPBT)$_2$]	–	1606m	1317m,	523m	437m
			1265m		
[Zn(HMPBT)$_2$]	–	1605m	1314m,	518m	427s
			1268m		

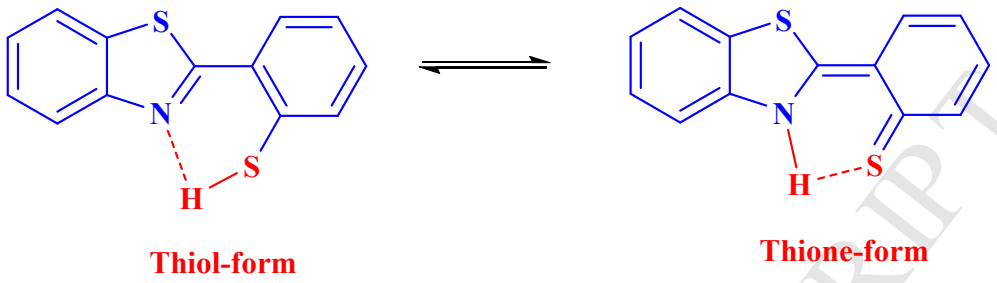

Figure 3. Proposed structure of ligand.

3.3. NMR spectral data

The ^{1}H NMR spectroscopic data of the ligand (Figure S5a) and its zinc complex (Figure S5b) have been recorded in DMSO-d6. In the NMR spectra of the metal complexes they indicate a shift of electron density from the ligand to the zinc atom. In the NMR spectra of the metal complexes they indicate a shift of electron density from the ligand to the zinc atom. The broad signal at 11.59 ppm is due to the –SH proton in ligand HMBT disappearance of the signal for spectrum of the –SH proton in the spectrum of the zinc complex supported the protonation of the thiol group. Spectrum of the ligand shows other signals in the range 8.17–6.98 ppm for aromatic protons. [^{1}H NMR (300 MHz, DMSO-d6) δ 8.08 (d, J = 8 Hz, 1H), 7.90 (d, J = 8 Hz, 1H), 7.68-7.61 (m, 2H), 7.47 (t, J = 8 Hz, 1H), 7.42-6.98 (m, 2H), 7.04 (dd, J = 8.4, 2 Hz, 1H), 11.59 (s, SH, 1H) for HMPBT ligand and (300 MHz, DMSO-d6) δ 8.07 (d, J = 8 Hz, 1H), 7.89 (d, J = 8 Hz, 1H), 7.67-6.98 (m, 2H), 7.47 (t, J = 8 Hz, 1H), 7.41-7.36 (m, 2H), 7.02 (dd, J = 8.17, 2 Hz, 1H), disapparance (s, SH, 1H) for Zn(II) complex].

The ^{13}C NMR spectrum of the ligand (Figure S6a) displayed characteristic signal at 154.0 ppm was due to –C=N carbon of the benzothiazole ring. The signal due to –C=N carbon was slightly shifted downfield in comparison to the corresponding signal of this group in the ligand thereby confirming the complexation with zinc metal ion (Figure S6b). **[**^{13}C NMR (75 MHz, DMSO-d6) *δ* 116.8, 118.8, 119.4, 121.8, 122.3, 125.2, 125.5, 126.7, 128.8, 132.3, 134.6, 151.5, 156.4, 165.6 for HMPBT ligand and ^{13}C NMR (75 MHz, DMSO-d6) *δ* 116.8, 118.8, 119.4, 121.8, 122.3, 125.2, 125.5, 126.7, 128.8, 132.3, 134.6, 151.5, 160.2,169.8 for Zn(II) complex].

3.4. Magnetic moment

The magnetic moments of the copper(II) and cobalt(II) complexes are 1.73 and 4.77 BM, respectively, which suggests square planar geometry for copper(II) complex and

tetrahedral geometry for cobalt(II) complex [38,39]. For tetrahedral cobalt(II) complex, the state acquires orbital angular momentum only indirectly through the mixing of the $^4T_2$ state by a spin–orbit coupling perturbation. The nickel(II) and zinc(II) complexes are diamagnetic at room temperature revealing the square planar and tetrahedral geometry for nickel(II) and zinc(II) complexes around the metal (II) ion [38].

3.5. Electronic spectra

The electronic spectra of the HMPBT ligand and its metal complexes are shown in Figure S7. Electronic absorption spectra of all the compounds were recorded in DMF solution over the range 200–800 nm at room temperature. The electronic spectra of the free ligand exhibits absorption bands at 216 and 287 nm, which are due to the intraligand π-π* transitions, these bands remain almost unchanged in the spectra of complexes [40]. Absorptions in the 362 nm is attributed to the n-π* transition associated with C=N, the bathochromic shift of this absorption upon complexation is due to the donation of a lone pair of electrons to the metal ion, indicating the coordination of (C=N) nitrogen of benzothiazole ring [40].

Cobalt (II) complex shows absorption bands at 14,948 cm^{-1} assigned to $^4A_2 \rightarrow {}^4T_1(P)$ transition. The existence of spin–orbit coupling also allows some quartet → doublet spin transition to occur. Another band at 14,124 cm^{-1} is assigned to $^4A_2 \rightarrow {}^4T_1$ (F). The expected $^4A_2 \rightarrow {}^4T_1$ transition appearing at a 4500 cm^{-1} is overlapped by ligand vibration transitions (i.e., the infrared bands) suggests tetrahedral geometry of the complex [41,42] which is also corroborated by magnetic moment value of the complex. Spectra of the nickel complex shows an absorption band at 15,263 cm^{-1}, assignable to a $^1A_1 \rightarrow {}^1A_2$ transition and a shoulder at 17,892 cm^{-1} corresponding to a $^1A_1 \rightarrow {}^1B_1$ transition which are consistent with square planar stereochemistry about the nickel(II) ion [42]. The visible spectrum of copper complex, shows two absorption bands at 14,970 cm^{-1} and 19,455 cm^{-1} assignable to $^2B_1 \rightarrow {}^2B_2$ and $^2B_1 \rightarrow {}^2E$ transitions respectively, which indicates the possibility of square planar geometry of the metal complex [43].

3.6. EPR spectrum of Cu(II) complex

The ESR spectra of the Cu(II) complex at room temperature (Table 3, Figure 4) exhibits anisotropic signals with g value $g_{\|}$ =2.242 and $g_{\perp}$= 2.071 (Table 4) which is characteristic for axial symmetry [44]. Since the $g_{\|}$ and $g_{\perp}$ values are closer to 2 and $g_{\|} > g_{\perp}$ suggesting a tetragonal distortion around the Cu(II) ion corresponding to elongation along the fourfold symmetry Z-axis [45]. The trend $g_{\|} > g_{\perp} > g_e$ (2.0023) shows that the unpaired electron is localized in the $dx^2–y^2$ orbital of the Cu(II) ion in complexes [46]. In addition, exchange coupling interaction between two Cu(II) ions is explained by Hathaway expression $G = (g_{\|} – 2)/(g_{\perp} – 2)$. When the value G< 4.0, a considerable exchange coupling is present in solid complex (G=1.686) [44]. Kivelson and Neiman showed that

for an ionic environment $g_{||}$ is normally 2.3 or larger, but for covalent environment $g_{||}$ are less than 2.3. The $g_{||}$ value for the Cu(II) complex is 2.242, consequently the environment is covalent.

The ESR spectra of the solid Co(II), Ni(II) and Zn (II) complexes at room temperature do not show ESR signal because the rapid spin lattice relaxation of the Co(II), and Ni(II) broadness the lines at higher temperatures [44] and the diamagnetic nature of the Zn(II) complex. The ESR spectra show signals that may be accounted for the presence of free radicals that can resulted from the cleavage of any double bond and distribution of the charge on the two neighbor atoms. The presence of unpaired electrons from any source inside the molecule can be responsible for the appearance of these signals.

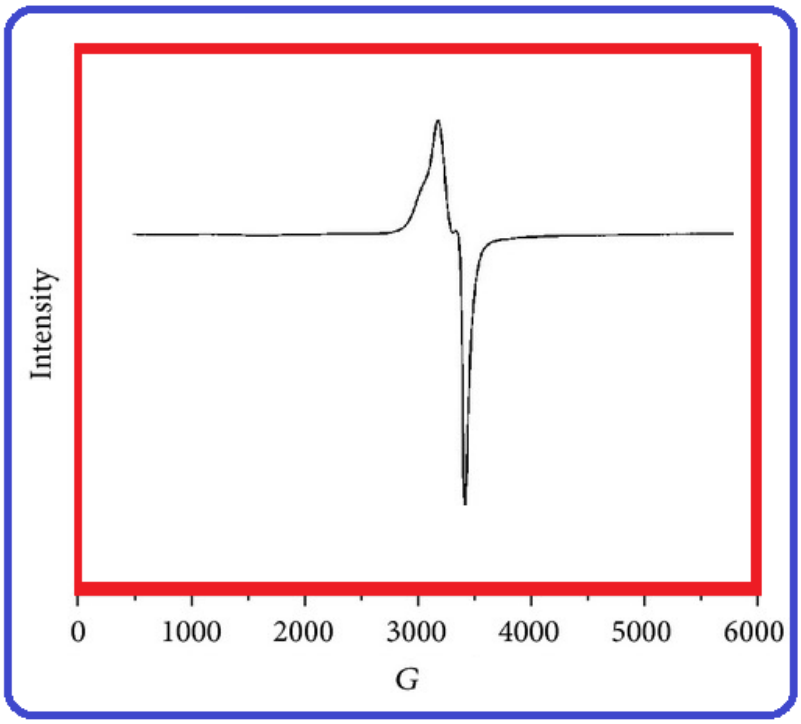

Figure 4. EPR spectrum of $[Cu(MPBT)_2]$ in polycrystalline state.

Table 3: ESR parameters of $[Cu(MPBT)_2]$ complex

Complex	$g_{\|}$	$g_{\perp}$	g_{iso}	$A_{\|} \times 10^{-4}$ (cm^{-1})	$g_{\|}/A_{\|}$	G
$[Cu(MPBT)_2]$	2.242	2.071	2.128	166.14	140	3.444

3.7. Thermal decomposition

The stages of decomposition, temperature range, decomposition product as well as the weight loss percentages of some metal complexes are given in Table 4. Figure 5 show the TGA curves of some metal complexes. The experimental weight loss values are in good

agreement with the calculated values. The final decomposition product was identified by the conventional chemical analysis method. [Co(MPBT)$_2$] complex is chosen as a representative example. In the TG thermogram of this complex, the first stage at 230–355 °C with weight loss of 13.92 (Calcd. 13.99%) is corresponding to the loss of carbon disulfide molecule. The second step with weight loss of 14.31 (Calcd. 14.36%) at 355–432 °C is attributed to the elimination of C_5H_4N fragments. The third step at 432–537 °C with weight loss of 10.29 (Calcd. 10.32%) is referring to the removal of $CH_3CN + CH_3$ molecules. The fourth step corresponds to the elimination of $C_{15}H_6S$ fragment with weight loss of 40.12 (Calcd. 40.15%). The residual part is CoO + 2C with weight loss 21.12(Calcd. 21.15%). An inspection of the data represented in Table 7 indicates that TG thermograms displayed a high residual part for the studied complexes reflecting a higher thermal stability [47, 48].

Table 4

Decomposition steps with the temperature range and weight loss for HMPBT complexes.

Compound (M.Wt.)	Decomposition step	Temperature range (°C)	Removes species	Wt. Loss % (Cald.)	%Found
[Co(MPBT)$_2$] (543.6)	1st	230–355	- CS_2	13.99	13.92
	2nd	355–432	- C_5H_4N	14.36	14.31
	3rd	432–537	- $CH_3CN + CH_3$	10.32	10.29
	4th	537-708	-$C_{15}H_6S$	40.15	40.12
	Residue	708-800	- CoS + 2C	21.15	21.12
[Ni(MPBT)$_2$] (543.4)	1st	228-352	- CS_2 + HCN	18.99	18.93
	2nd	352-433	- C_5H_4N	30.21	30.17
	3rd	433-530	-$C_{13}H_8$	14.37	14.36
	4th	530-697	-C_4H_3S	15.29	15.27
	Residue	697-800	-NiS+ 2C	21.12	21.16
[Cu(MPBT)$_2$] (548.2)	1st	230-364	- CS_2 + HCN	18.82	17.97
	2nd	364-442	- H_2S	6.22	6.21
	3rd	442-543	- C_5H_4N	14.24	14.22
	4th	543-703	- $C_{16}H_9$	36.70	36.63
	Residue	703-800	- CuS + 3C	24.00	23.11
	1st	232-368	-CS_2 + H_2S	20.03	19.93
	2nd	368-444	-HCN	4.90	4.87

Compound (M.Wt.)	Decompositi on step	Temperatue range (°C)	Removes species	Wt. Loss % (Cald.)	%Found
$[Zn(MPBT)_2]$ (550)	3rd	444-547	- C_5H_5N	14.38	14.32
	4th	547-706	-$C_{11}H_8$	25.49	25.44
	Residue	706-800	-ZnS+8C	35.18	35.15

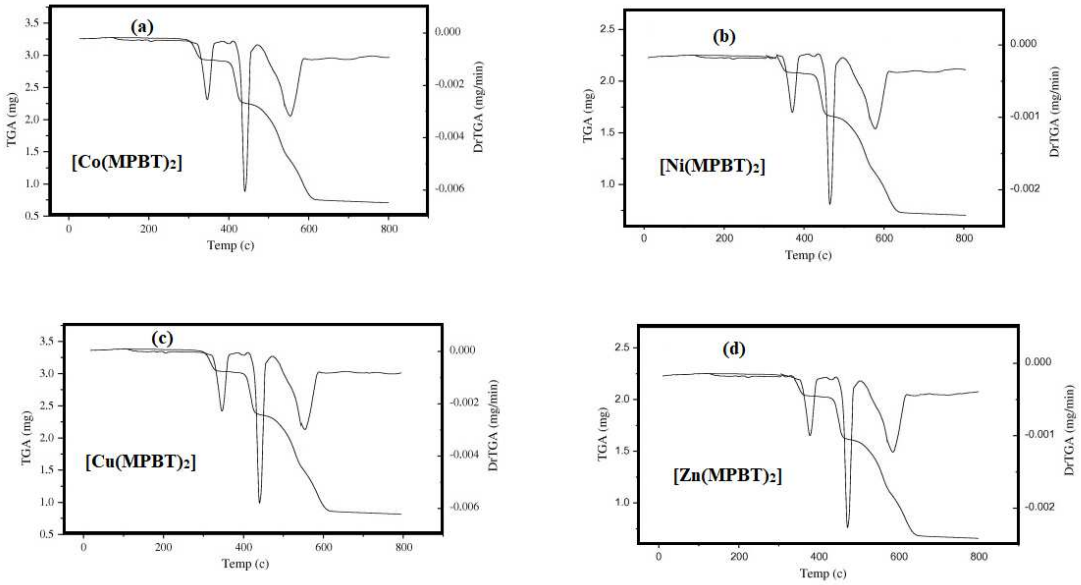

Figure 5. Thermal analysis curves (TGA and DTG) of Co(II), Ni, Cu(II) and Zn(II) complexes.

3.8. Kinetic studies

The thermodynamic activation parameters of decomposition processes of the metal (Co(II), Ni(II), Cu(II) and Zn(II)) complexes namely activation energy (*E**), entropy (Δ*S**) and Gibbs free energy change of the decomposition (Δ*G**) were evaluated graphically by employing three methods, Coats–Redfern [49] (CR), Horowitz–Metzger [50] (HM) and Piloyan–Novikova [51] (PN). The data are summarized in Tables 5–7. From the results obtained, the following remarks can be pointed out:

(1) The energy of activation (E) values increases on going from one decomposition stage to another for a given complex, indicating that the rate of decomposition decreases in the same order. Generally stepwise stability constants decrease with an increase in the number of ligand attached to a metal ion. Conversely, during decomposition reaction the rate of removal of remaining ligands will be smaller after the expulsion of furan-Schiff's base ligand (H-MPBT).

(2) The ΔG values increases significantly for the subsequently decomposition stages due to increasing the TΔS values from one stage to another. This may be attributed to the structural rigidity of the remaining complex after the expulsion of more ligands, as compared with the precedent complex, which require more energy, TΔS, for its rearrangement before undergoing any compositional change.

(3) The ΔS negative values for the decomposition steps indicate that all studied metal(II) complexes are more ordered in their activated states.

(4) The ΔH positive values mean that the decomposition processes are endothermic.

(5) The activation energies of decomposition were found to be in the range 137.33–147.99 kJ mol^{-1}.

(6) The linearization plots (Figure 6), confirms the first-order kinetics for the decomposition process (Coats-Redfern method).

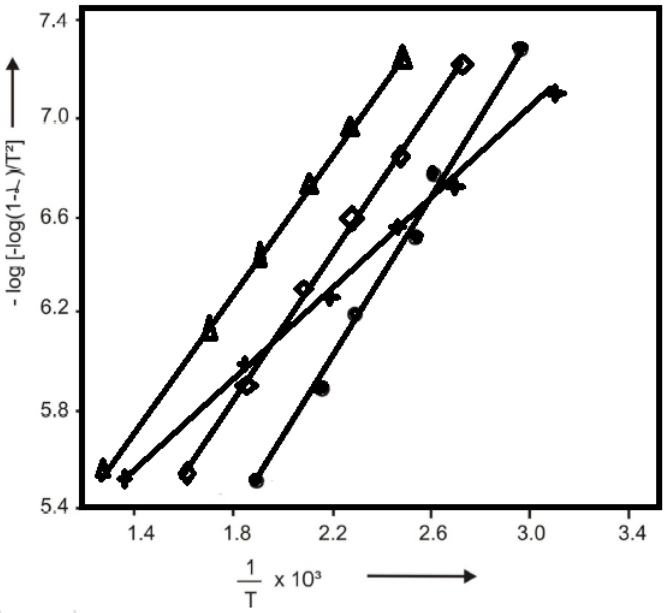

Figure 6. Linearization plot of (a) (●) $[Co(MPBT)_2]$ complex, (b) (◊) $[Ni(MPBT)_2]$ complex, (c) (♦) $[Cu(MPBT)_2]$ complex, and (d) (▲) $[Zn(MPBT)_2]$ complex.

Table 5
Kinetic Parameters evaluated by Coats–Redfern equation for the metal complexes.

Complex	Peak	Mid Temp(K)	Ea KJ\mol	A (S^{-1})	ΔH* KJ\mol	ΔS* KJ\mol.K	ΔG* KJ\mol
$[Co(MPBT)_2]$	1^{st}	404.8	65.84	$1.26x10^5$	42.28	-0.1523	75.36

	2nd	625.4	89.25	$1.18x10^5$	87.47	-0.1678	123.24
	3rd	743.6	172.23	$1.23x10^7$	123.52	-0.0882	188.69
	4th	896.8	223.54	$6.86x10^8$	167.88	-0.0584	235.12
$[Ni(MPBT)_2]$	1st	406.3	36.58	$2.82x10^4$	43.13	-0.1769	89.53
	2nd	589.8	68.69	$1.56x10^5$	67.42	-0.1458	115.34
	3rd	648.9	164.46	$3.23 x10^8$	134.56	-0.0653	136.47
	4th	898.7	178.23	$1.33x10^9$	179.98	-0.0583	188.23
$[Cu(MPBT)_2]$	1st	415.6	78.87	$2.64 x10^{10}$	46.82	-0.0147	115.36
	2nd	546.1	112.35	$2.14 x10^6$	86.23	-0.1022	145.75
	3rd	721.3	136.96	$1.83 x10^7$	123.54	-0.1189	182.82
	4th	978.6	189.99	$2.28 x10^8$	176.69	-0.1008	237.49
$[Zn(MPBT)_2]$	1st	472.3	86.08	$2.68x10^7$	56.53	-0.0575	101.76
	2nd	688.7	154.13	$1.32x10^9$	88.42	-0.0402	168.27
	3rd	769.4	187.46	$2.24x10^{10}$	122.23	-0.0323	210.34
	4th	937.6	216.87	$2.33x10^{11}$	146.87	-0.0089	248.08

Table 6
Kinetic Parameters evaluated by Horowitz-Metzger equation for the metal complexes.

Complex	Peak	Mid Temp(K)	Ea KJ\mol	A (S^{-1})	ΔH* KJ\mol	ΔS* KJ\mol.K	ΔG* KJ\mol
$[Co(MPBT)_2]$	1st	404.8	65.58	$1.38x10^5$	42.56	-0.1421	75.82
	2nd	625.4	89.13	$1.22x10^5$	87.52	-0.1358	123.67
	3rd	743.6	172.11	$1.46x10^7$	123.88	-0.0975	188.73
	4th	896.8	223.12	$6.85x10^8$	168.21	-0.0645	235.19
$[Ni(MPBT)_2]$	1st	406.3	36.86	$2.35x10^4$	43.36	-0.1803	89.46
	2nd	589.8	68.74	$1.71x10^5$	67.75	-0.1533	115.91
	3rd	648.9	164.33	$3.37 x10^8$	134.66	-0.0820	136.43
	4th	898.7	178.78	$1.36x10^9$	1180.23	-0.0457	188.48
$[Cu(MPBT)_2]$	1st	415.6	78.67	$2.47 x10^{10}$	47.12	-0.0143	115.58
	2nd	546.1	112.44	$2.58 x10^6$	86.45	-0.1001	145.98
	3rd	721.3	136.89	$1.63 x10^7$	123.36	-0.9247	182.82
	4th	978.6	189.47	$2.47 x10^8$	176.24	-0.0663	237.57
$[Zn(MPBT)_2]$	1st	472.3	86.24	$2.58x10^7$	56.48	-0.0862	101.88
	2nd	688.7	154.48	$1.67x10^9$	88.63	-0.0642	168.74
	3rd	769.4	187.71	$2.42x10^{10}$	122.34	-0.0475	210.56
	4th	937.6	217.03	$2.75x10^{11}$	147.14	-0.0334	248.45

Table 7
Kinetic Parameters evaluated by Piloyan–Novikova equation for the metal complexes.

Complex	Peak	Mid Temp(K)	Ea KJ\mol	A (S^{-1})	ΔH* KJ\mol	ΔS* KJ\mol.K	ΔG* KJ\mol

$[Co(MPBT)_2]$	1st	404.8	66.12	$2.42x10^5$	41.83	-0.1578	76.12
	2nd	625.4	89.74	$1.75x10^5$	87.19	-0.1669	124.08
	3rd	743.6	172.68	$2.03x10^7$	123.62	-0.0892	188.75
	4th	896.8	223.84	$6.98x10^8$	167.24	-0.0587	235.35
$[Ni(MPBT)_2]$	1st	406.3	37	$2.65x10^4$	43.25	-0.1774	89.87
	2nd	589.8	69.11	$1.72x10^5$	67.46	-0.1491	115.66
	3rd	648.9	164.52	$3.42\ x10^8$	134.84	-0.0667	136.48
	4th	898.7	178.83	$1.82x10^9$	180.42	-0.0582	187.72
$[Cu(MPBT)_2]$	1st	415.6	79.24	$2.83\ x10^{10}$	46.93	-0.0152	115.58
	2nd	546.1	112.47	$2.18\ x10^6$	86.28	-0.1046	145.92
	3rd	721.3	137.26	$2\ x10^7$	123.94	-0.1178	182.73
	4th	978.6	191.34	$2.36\ x10^8$	176.73	-0.0728	237.16
$[Zn(MPBT)_2]$	1st	472.3	85.67	$2.89x10^7$	56.22	-0.0537	101.73
	2nd	688.7	154.89	$1.46x10^9$	88.88	-0.0481	168.28
	3rd	769.4	187.39	$2.32x10^{10}$	122.59	-0.0284	210.23
	4th	937.6	216.92	$2.41x10^{11}$	146.94	-0.0087	247.75

3.9. Powder XRD

Single crystals of the complexes could not be prepared to get the XRD and hence the powder diffraction data were obtained for structural characterization. Structure determination by X-ray powder diffraction data has gone through a recent surge since it has become important to get to the structural information of materials, which do not yield good quality single crystals. The indexing procedures were performed using (CCP4, UK) CRYSFIRE program [52–55] giving orthorhombic crystal system for $[Co(MPBT)_2]$ (Figure 7a) having M(9) = 8, F(6) = 7, orthorhombic crystal system for $[[Ni(MPBT)_2]$ (Figure 7b) having M(9) = 9, F(6) = 8, monoclinic crystal system for $[Cu(MPBT)_2]$ (Figure 7c) having M(6) = 11, F(6) = 7 and monoclinic crystal system for $[Zn(MPBT)_2]$ (Figure 7d) having M(6) = 10, F(6) = 6, as the best solutions. Their cell parameters are shown in Table 8.

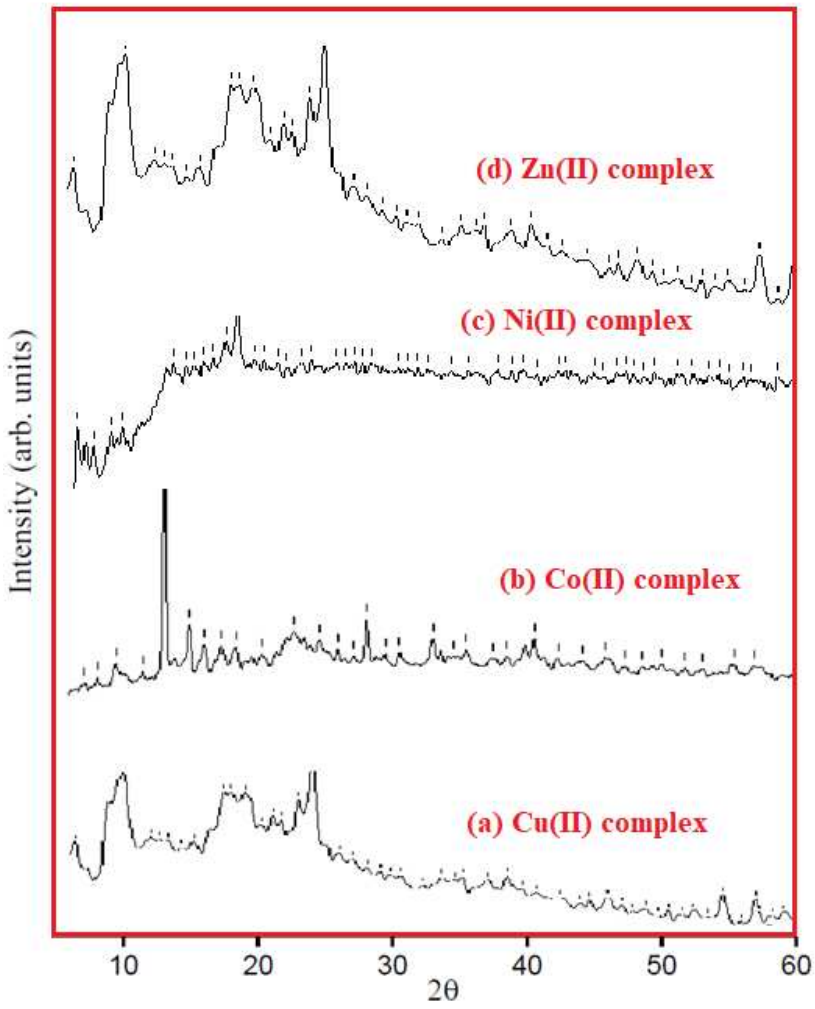

Figure 7. Powder X-ray diffraction patterns of Co(II), Ni(II), Cu(II) and Zn(II) complexes in the range of 2–60° (2θ).

Table 8
Crystallographic data for the Schiff's base complexes $[Cu(MPBT)_2]$, $[Co(MPBT)_2]$, $[Ni(MPBT)_2]$ and $[Zn(MPBT)_2]$.

Crystal data	**$[Cu(MPBT)_2]$**	**$[Co(MPBT)_2]$**	**$[Ni(MPBT)_2]$**	**$[Zn(MPBT)_2]$**
Empirical formula	$C_{26}H_{16}N_2S_4Cu$	$C_{26}H_{16}N_2S_4Co$	$C_{26}H_{16}N_2S_4Ni$	$C_{26}H_{16}N_2S_4Zn$
Formula mass	548.2	543.6	543.4	550.0
Crystal system	orthorhombic	orthorhombic	monoclinic	monoclinic
Space group	Pbn21	P21 21 21	P121/n1	P121/c1
a [Å]	6.4231(7)	6.7415(2)	5.8080(2)	14.8293(10)
b [Å]	18.605319)	13.2986(4)	17.5649(7)	13.5103(8)
c [Å]	23.8794(2)	16.1145(5)	18.6047(7)	9.9645(7)
α [°]	90	90	90	90
β [°]	90	90	90.788(3)	100.468(5)
γ [°]	90	90	90	90

V [Å^3]	2934.528(5)	15.564(8)	1878.649(12)	1821.264(2)
Z	1	4	4	4
ρ_{calc} [g cm^{-3}]	1.512	1.503	1.362	1.378
μ [mm^{-1}]	0.253	0.247	0.184	0.199
F(000)	1406	969	897	846
θ_{min}-θ_{max} [º]	2.27-29.24	2.73- 28.47	1.67-27.78	1.32-27.72
T/K	296(2)	296.(2)	296(2)	296(2)
Index range	$-7 \le h \le 8$	$-9 \le h \le 8$	$-8 \le h \le 8$	$-16 \le h \le 19$
	$-25 \le k \le 23$	$-18 \le k \le 18$	$-21 \le k \le 21$	$-14 \le k \le 18$
	$-32 \le l \le 32$	$-20 \le l \le 20$	$-25 \le l \le 24$	$-13 \le l \le 13$
Collected reflections	6873	3398	4358	4527
Unique reflections	3628	2249	2208	2213
Refined parameters	428	231	248	288
R1, wR2	0.0552, 0.1437	0.0454, 0.0978	0.0675, 0.1887	0.0554, 0.1478

3.10. Antimicrobial activity

All the compounds were evaluated for their antibacterial activity in vitro by using zone inhibition technique against *P. aeriginosa , S. aureus, B. subtilis*, and *E. coli*. Experiments were repeated three times and the results were expressed as values in Figure 8, Table 9. The results obtained were compared with the standard drugs streptomycin and captan. All the compounds showed antimicrobial activity against *B. Subtilis*. The table shows that compounds Ni(II), Cu(II) and Zn(II) exhibited significant activity against *E. coli* and *S. aureus* respectively.

Table 9. Inhibition diameter in millimeters of Schiff's base (HMPBT) and its complexes.

Compound	*P.aeriginosa*	*S. aureus*	*B. subtilis*	*E. coli*	Streptomycin	Captan
HMPBT	0	0	13	13	26	23
$[Co(MPBT)_2]$	0	0	9	10	22	26
$[Ni(MPBT)_2]$	8	10	11	16	25	30
$[Cu(MPBT)_2]$	0	8	9	10	26	23
$[Zn(MPBT)_2)]$	10	10	9	11	25	27

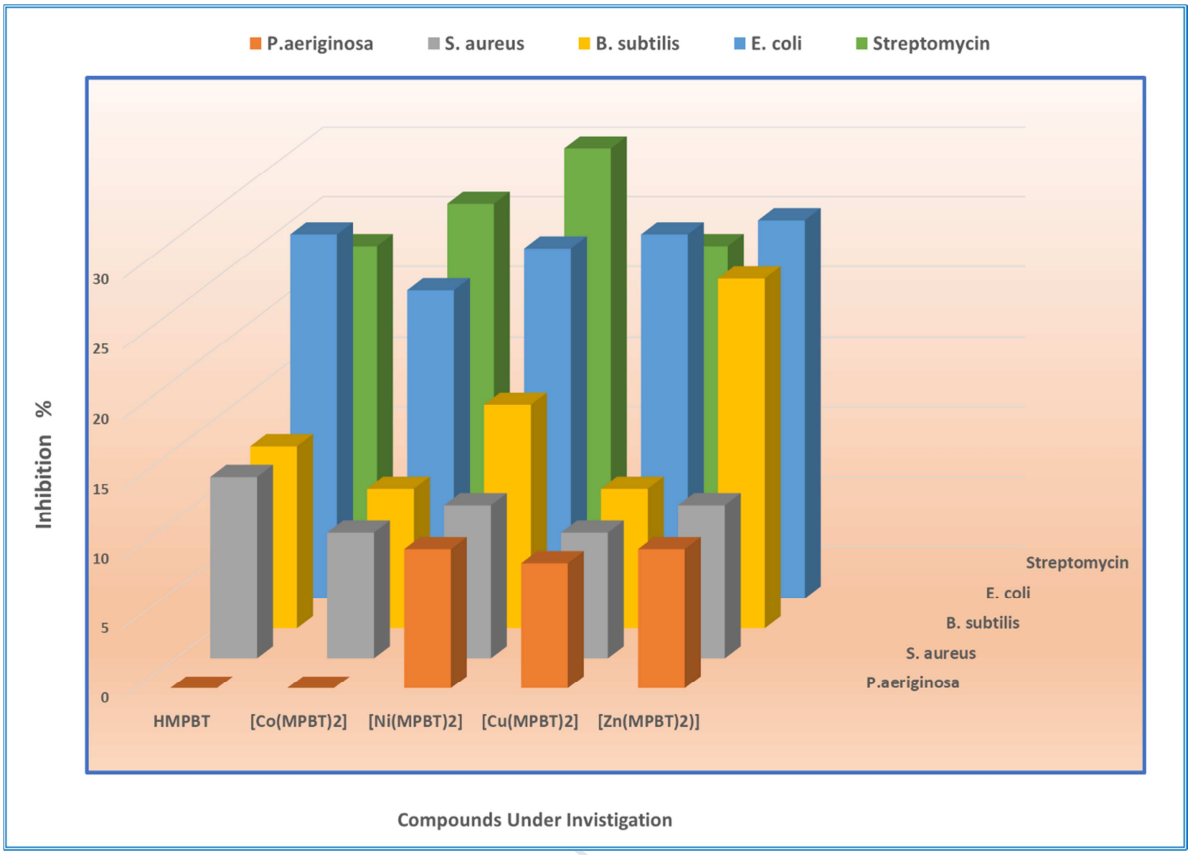

Figure 8. Graph showing antibacterial behavior of compounds against *P. aeriginosa* , *S. aureus*, *B. subtilis*, and *E. coli* of HMPBT ligand and its complexes.

5. DNA-Binding Studies

5.1. Absorption and Fluorescence Spectroscopy Studies

In order to investigate DNA-binding of Zn(II) complex, the absorption titration was performed between the range of 300 to 800 nm wavelengths. The UV/Vis spectra of Zn(II) complex in DMF give peaks at around 670 and 640 nm for Q-band absorption and around 350 nm for B-band absorption in the absence of CT-DNA. The absorption spectra of Zn(II) complex given in Figure 9 indicated hypochromic and red changes in the presence of CT-DNA. In the presence of CT-DNA, as the concentration of CT-DNA was enhanced from 0 to 3 µM, a strong hypochromic shift was observed with a small change in wavelength. The substantial hypochromic shifts suggest that a strong interaction takes place between Zn(II) complex and CT-DNA. These results show that Zn(II) complex binds to CT-DNA via intercalative binding mode.

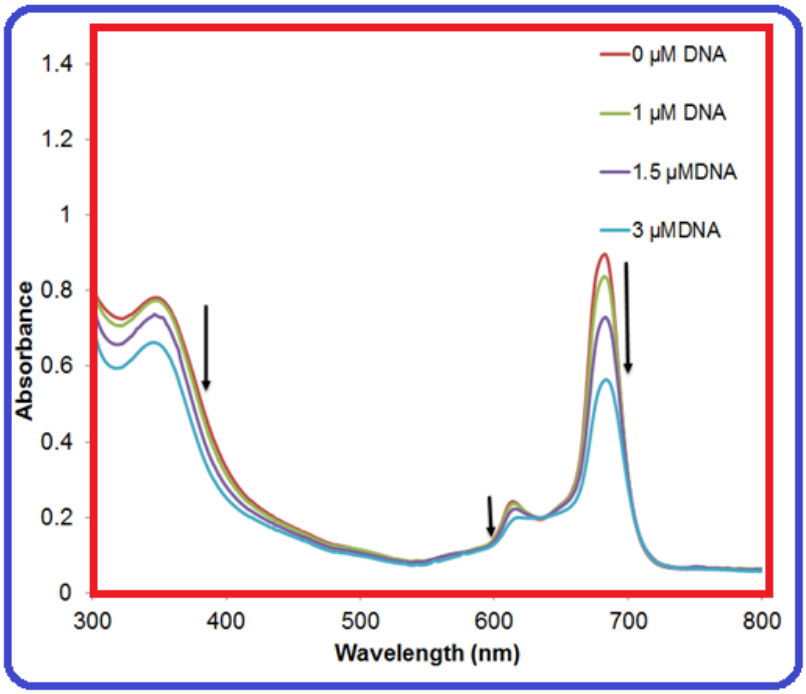

Figure 9. Absorption spectra of Zn(II) complex in Tris -HCI buffer (pH 7.0) upon increasing concentration of CT-DNA. Arrows show the absorbance change on increasing concentration of CT-DNA.

A fluorescence titration technique is a common and sensitive method in DNA-binding studies, it can provide further information on the interaction between CT-DNA and metallo compound. A fluorescence titration study is conducted to determine the interaction between DNA and metal complexes. In the absence and the presence of CT-DNA, fluorescence titration study was carried out to investigate the binding activities between DNA and Zn(II) complex. As indicated in Figure 10, in the absence of CT-DNA, Zn(II) complex scatters strong emissions in a Tris-HCl buffer solution (pH 7.0) at room temperature with a peak appearance at around 565 nm. On the addition of CT-DNA, a clear increase in emission intensities of Zn(II) complex was observed compared to the original Zn(II) complex, as shown in Figure 3. In the presence of CT-DNA, Zn(II) complex gives emissions at around 579 nm. The results show that Zn(II) complex interacts strongly with CT-DNA in a Tris-HCl buffer at pH 7.0.

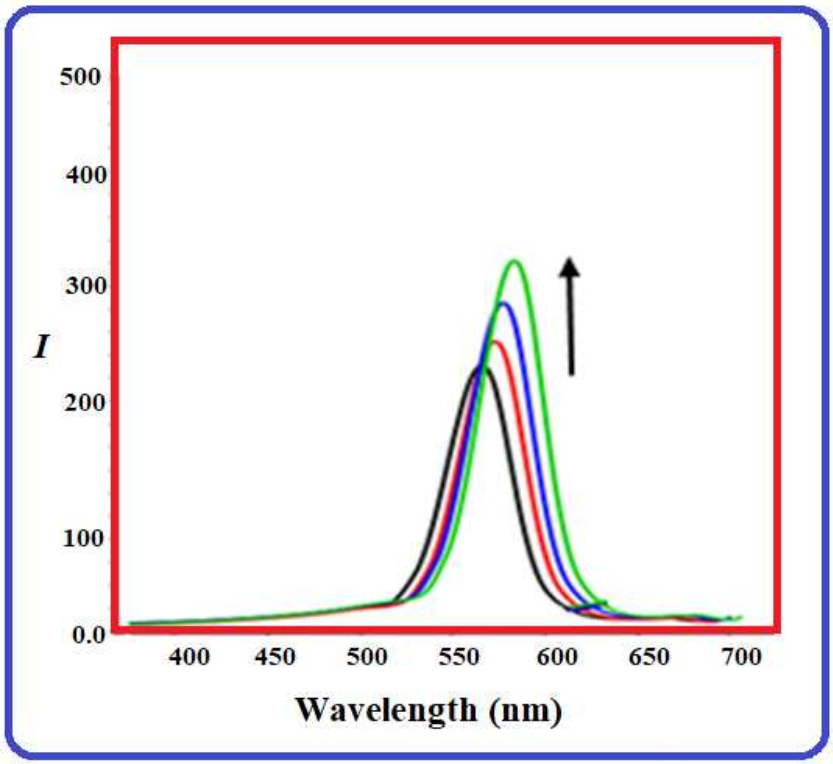

Figure 10. Fluorescence emission spectra of Zn(II) complex in Tris -HCI buffer (pH 7.0) in the absence and the presence of CT-DNA. Arrow shows the intensity change on increasing CT-DNA concentrations, where *I* is intensity.

5.2. Cyclic Voltammetry Studies

In this study, in the absence and the presence of CT-DNA, cyclic voltammetric studies were conducted to understand the interaction between CT-DNA and Zinc(II) complex in a Tris-HCl buffer at pH 7.0 and the findings are indicated in Figure S8. In the absence of CT-DNA, Zn(II) complex produces a couple of waves belonging to Zinc(II) complex showing the cathodic (EPc) and anodic peak potential (EPa). The cathodic (EPc) and anodic peak (EPa) potential were determined to be −0.23 V (EPc) and −0.53 V and 0.14 V (EPa) for Zn(II) complex as shown in Figure S8. In the presence of CT-DNA, upon the addition of CT-DNA with Zn(II) complex, the cyclic voltammetric peak currents dropped significantly. This result indicates that CT-DNA interacts with Zn(II) complex. The decrease of the voltammetric peak currents in the presence of CT-DNA can be attributed to the low diffusion of Zn(II) complex binding to CT-DNA molecules. In the presence of CT-DNA, the cathodic peak potential (EPc) and anodic peak potential (EPa) were recorded to be –0.3 V (EPc) and –0.69 V and 0.11 V (EPa) for Zn(II) complex as shown in Figure S8. All these findings indicate that Zn(II) complex binds to CT-DNA.

5.3. DNA cleveage Studies

In this work, a gel electrophoresis experiment, was performed on the interaction of the DNA with Zn(II) complex at room temperature using CT-DNA in the absence and presence of the synthesized Zn(II) complex. The ability to bind the synthesized Zn(II) complex with CT-DNA was examined by agarose gel electrophoresis to investigate the impact of different amounts of Zn(II) complex upon the CT-DNA. The findings are shown in Figure S9. It is explicitly shown that the intensity of the DNA bands was decreased after interaction of Zn(II) complex with CT-DNA when compared to the control CT-DNA (C). The decrease in the intensity of CT-DNA bands after the interaction of Zn(II) complex with CT-DNA is thought to be due to the deformation of the double-stranded DNA. The gel electrophoresis experiments clearly demonstrated that Zn(II) complex interacted with CT-DNA as there was a change in the bands in lanes 1 to 3, compared to the control CT-DNA (C) given in Figure 7. Lanes 1, 2 and 3 belong to Zn(II) complex and lane C belongs to the control CT-DNA**.** The binding ability of Zn(II) complex was compared to that of the control DNA (C), is due to its efficient CT-DNA binding ability. As indicated in Figure S9, it was observed that the control CT-DNA band did not show any remarkable change in the lane C band. It was clearly seen that Zn(II) complex interacted with CT-DNA when compared with the control CT-DNA (C). In addition, the interaction of Zn(II) complex with the DNA caused partial neutralization of the DNA bands. The presence of a smear in the gel diagram indicated the cleavage, as shown in Figure S9, and the cleavage effect of Zn(II) complex is comparable to that of the C band due to their effective DNA-interaction ability. As a result, the interaction of Zn(II) complex with CT-DNA causes partial neutralization of CT-DNA bands. These results demonstrated that Zn(II) complex could strongly interact with CT-DNA.

6. Conclusion

The structures of the complexes of HMPBT with Co(II), Ni(II), Cu(II) and Zn(II) ions are confirmed by the elemental analyses, IR, ^{1}H NMR, molar conductance, magnetic moment, UV–VIS., ESR and thermal analyses data. Therefore, from the IR spectra, it is concluded that HMPBT behaves as a ligand bidentate ligand with two NS sites coordinating to the metal ions via the benzothiazole N ring, and deprotonated thiolic–S group. From the molar conductance data of the complexes (Λ_m), it is concluded that the complexes of HMPBT ligand are considered as non-electrolytes. The ^{1}H NMR spectra of the free ligand shows that the SH signal, appeared in the spectrum of HL ligand at 11.59 ppm completely disappeared in the spectra of its Zn(II) complex indicating that the SH proton is removed by the chelation with Zn(II) ion. Geometry optimization and conformational analysis have been performed and the perfect agreement with spectral studies allows for suggesting the exact structure of all studies complexes. The stability of complexes was explained and kinetic parameters (Ea, A, ΔH, ΔS and ΔG) of all the thermal decomposition stages have been evaluated using Coast-Redfern, Horowitz–

Metzger (HM), and Piloyan–Novikova (PN) methods. On the basis of the above observations and from the magnetic and solid reflectance measurements, square planar geometry for Cu(II) and Ni(II) complexes and tetrahedral geometry for Co(II) and Zn(II) complexes is suggested for the investigated complexes. The structure of the complexes is shown in Scheme 2. The investigated ligand and metal complexes were screened for their *in-vitro* antimicrobial activities against different types of fungal and bacterial strains. The resulting data assert on the inspected compounds as a highly promising bactericides and fungicides.

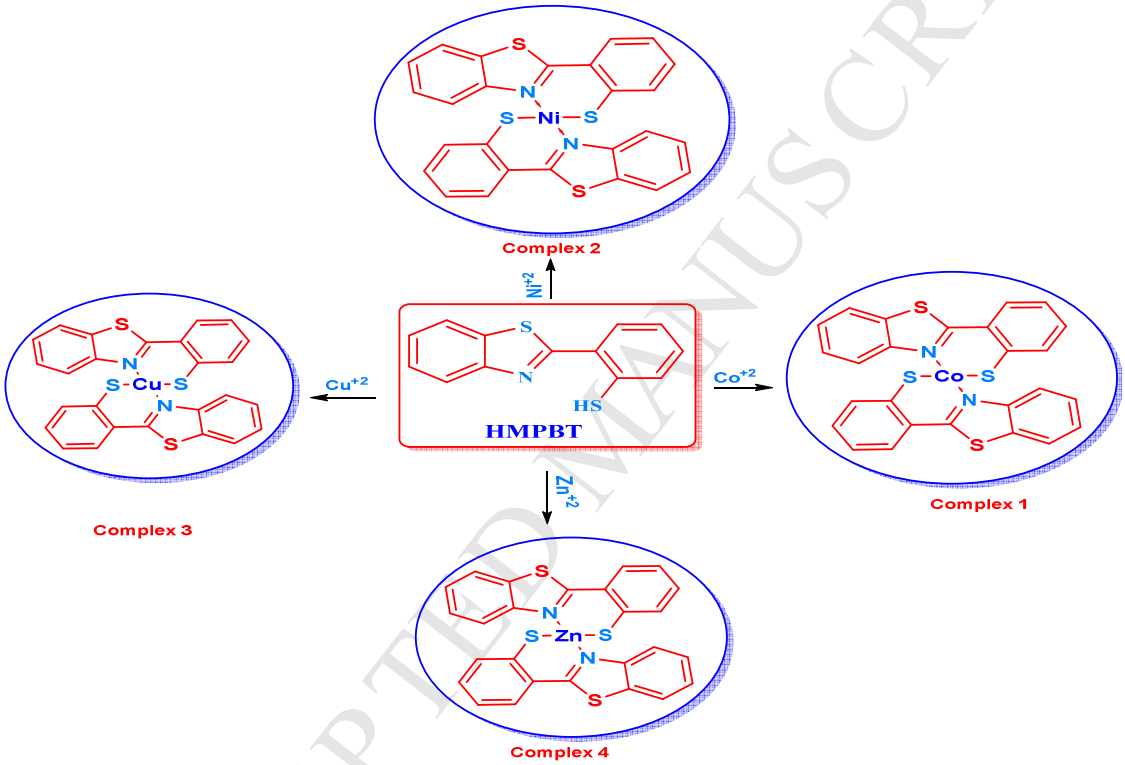

Scheme 2. Synthesis of metal complexes from HMPBT with Co(II), Ni(II), Cu(II), and Zn(II) ions.

Acknowledgements

"This work was funded by the Deanship of Scientific Research at Princess Nourah bint Abdulrahman University, through the Research Groups Program Grant no. (RGP-1438-00....)".

References

[1] Y. Sun, D.L. Smith, R.E. Shoup, Anal. Biochem. 197 (1991) 69–76.
[2] M. Cappiello, P.G. Vilardo, V. Micheli, G. Jacomelli, S. Banditelli, V. Leverenz, F.J. Giblin, A. del Corso, U. Mura, Exp. Eye Res. 70 (2000) 795–803.
[3] L.A. Bumm, J.J. Arnold, M.T. Cygan, T.D. Dunbar, T.P. Burgin, L. Jones, D.L. Allara, J.M. Tour, P.S. Weiss, Science 271 (1996):1705–1707.
[4] F. Schreiber, Prog. Surf. Sci. 65 (2000) 151–257.
[5] W.L. Banwart, J.M. Bremner, Soil Biol. Biochem. 7 (1975)359–364.
[6] G.A. Jeffrey, An introduction to hydrogen bonding. Oxford University Press, New York, (1997).
[7] H. Raissi, M. Yoosefian, F. Mollania, Int. J. Quantum Chem. 112 (2012) 2782–2786.
[8] B. Kuhn, P. Mohr, M.Stahl, J. Med. Chem. 53 (2010) 2601–2611.
[9] G. Zhao, F. Yu, M. Zhang, B. Northrop, H. Yang, P. Han K, Stang, J. Phys. Chem. A 115 (2011) 6390–6393.
[10] X. Cao, C. Liu, Y. Liu, Theor Comput Chem 11 (2012) 573–586.
[11] F.M. Raymo, M.D. Bartberger, K.N. Houk, J.F. Stoddart, J. Am. Chem. Soc. 123 (2001) 9264–9267.
[12] G.J. Zhao, K.L. Han, Acc. Chem. Res. 45 (2012) 404–413.
[13] Materials studio v 5.0, copyright Accelrys software Inc., 2009.
[14] W.J. Hehre, L. Radom, P.V.R. Schlyer, J.A. Pople, *Ab* Initio Molecular Orbital Theory, Wiley, New York, 1986.
[15] A. Kessi, B. Delley, Int. J. Quantum Chem. 68 (1998) 135–144.
[16] B. Hammer, L.B. Hansen, J.K. Nørskov, Phys. Rev. B 59 (1999) 7413–7421.
[17] A. Matveev, M. Staufer, M. Mayer, N. Rösch, Int. J. Quantum Chem. 75 (1999) 863–873.
[18] Z.H. Chohan, Chem. Pharm. Bull. 39 (1991) 1578–1580.
[19] A. Wolfe, G.H. Shimer, T. Meehan, Biochem. 26 (1987) 6392-6396.
[20] N.C. Lopez Zeballos, G.A. Gauna, M.C. Garcia Vior, J. Awruch, L.E. Dicelio, J. Photochem. Photobiol. B 136 (2014) 29-33.
[21] M. Özçesmeci, Ö.B. Ecevit, S. Sürgün, S. Humuryudan, Dyes Pigm. 96 (2013) 52-58.
[22] N. Demirezen, D. Tarınc, D. Polat, M. Cesme, A. Golcu, M. Tumer, Spectrochim. Acta A 94 (2012) 243-255.
[23] S. Sagdinc, B. Koksoy, F. Kandemirli, S.H. Bayari, J. Mol. Struct. 917 (2009) 63–70.
[24] I. Obot. N. Obi,. Der Pharma Chemica; 1 1 (2009) 106-123.
[25] E.B. Ottis "hazardous materials" Nova Science Publishers, Inc. (2006).
[26] T. Lemi,T. The Scientific World Journal Volume, Article ID 526289 (2012).

[27] M.J. Ajay, "density functional theory (DFT) study of reaction pathways on gold" (2007) 47
[28] K. Chandrakumar, P. Sourav. Int. J. Molec. Sci. 3 (2002) 324-337.
[29] P. Comba, T.W. Hambley, "Molecular Modeling of Inorganic Compounds", VCH, Weinheim (1995).
[30] D.X. West, J.K. Swearingen, J. Valdés-Martinez, S. Hernández-Ortega, A.K. El-Sawaf, F.v. Meurs, A. Castiñeiras, I. Garcia, E. Bermejo, Polyhedron 18 (1999) 2919–2929.
[31] A.A.R. Despaigne, J.G. Da Silva, A.C.M. Do Carmo, F. Sives, O.E. Piro, E.E. Castellano, H. Beraldo, Polyhedron 28 (2009) 3797–3803.
[32] W.J. Hehre, A.J. Shusterman, W.W. Huang, "A Laboratory Book of Computational Organic Chemistry", Wavefunction Inc, USA, 1996.
[33] M. Tyagi, S. Chandra, P. Tyagi, Spectrochim. Acta A 117 (2014) 1–8.
[34] J. Joseph, G.B. Janaki, J. Mol. Struct. 1063 (2014) 160–169.
[35] P.P. Netalkar, S.P. Netalkar, S. Budagumpi, V.K. Revankar, Eur. J. Med. Chem. 79 (2014) 47–56.
[36] J.C.T. Rendell, L.K. Thompson, Can. J. Chem. 57 (1979) 1–7.
[37] W. Freinbichler, A. Soliman, R.F. Jameson, G.N.L. Jamesond, W. Linert, Spectrochim. Acta A 74 (2009) 30–35.
[38] B.K. Singh, U.K. Jetley, R.K. Sharma, B.S. Garg, Spectrochim. Acta A 68 (2007) 63–73.
[39] B.N. Figgs, Introduction to Ligand Fields, 1st ed., 1966.
[40] D.H. Williams, I. Flemings, Spectrophotomtric Methods in Organic Chemistry, 4th ed., McGraw-Hill, London, 1989.
[41] M. Ciampolini, Struct. Bonding 6 (1969) 52–93.
[42] K. Nakamoto, S.J. McCarthy, Spectroscopy & Structure of Metal Chelate Compounds, John Wiley & Sons, USA, 1968.
[43] T.P. Chessman, D. Hall, T.N. Waters, J. Chem. Soc. A (1966) 694-695.
[44] M.F.R. Fouda, M.M. Abd-el-zaher, M.M.E. Shadofa, F.A. El Saied, M.I. Ayad, A.S. El Tabl, Trans. Met. Chem. 33 (2008) 219–228.
[45] S. Chandra, U. Kumar, Spectrochim. Acta A 61 (2005) 219–224.
[46] K.B. Gudasi, S.A. Patil, R.S. Vadavi, R.V. Shenoy, Trans. Met. Chem. 31(2006) 586–592.
[47] S. Bal, J.D. Connolly, Arab. J. Chem. http://dx.doi.org/10.1016/ j.arabjc.2015.11.012 (2015).
[48] R.K. Jain, A.P. Mishra, P. Gupta, J. Therm. Anal. Calorim. 2012 (110) (2012) 529–534.
[49] A.W. Coats, J.P. Redfern, Nature 20 (1964) 68–69.
[50] H.H. Horowitz, G. Metzger, Anal. Chem. 35 (1963) 1464–1468.
[51] G.O. Piloyan, T.D. Pyabonikar, C.S. Novikova, Nature, 212 (1966) 1229–1304.

[52] R. Shirley, The CRYSFIRE System for Automatic Powder Indexing: UsersManual, Lattice Press, 2002.
[53] A.M.A. Alaghaz, M.E. Zayed, S.A. Alharbi, R.A.A. Ammar, A. Chinnathambi, J. Molecu. Struct. 1087 (2015) 60–67.
[54] R.A. Ammar, A.M.A. Alaghaz, M.E. Zayed, L.A. AL-Bedair, J. Molecu. Struct. 1141 (2017) 368–381.
[55] S.I. Al-Saeedi, A.M.A. Alaghaz, R.A. Ammar, J. Molecu. Struct. 1111 (2016) 1–13.

Highlights

Title: Synthesis, spectral characterization, Quantum Chemical calculations, in-vitro antimicrobial and DNA activity studies of 2-(2'-mercaptophenyl) benzothiazole complexes

Reda A. Ammar [a], Amani S. Alturiqi [b], Abdel-Nasser M.A. Alaghaz [c,d] and Mohamed E. Zayed[e]

[a] Department of Chemistry, College of Science, Al-Imam Mohammad Ibn Saud Islamic University (IMSIU), 13623 Riyadh, Saudi Arabia.
[b] Department of Chemistry, College of Science, Princess Nourah bint Abdul Rahman University, Saudi Arabia.
[c] Department of Chemistry, Faculty of Science, Jazan University, Jazan, Saudi Arabia.
[d] Department of Chemistry, Faculty of Science (Boys), Al-Azhar University, Cairo, Egypt.
[e] Department of Botany and Microbiology, Faculty of Science, King Saud University, Riyadh 11541, Saudi Arabia

highlights

► Novel Schiff base (HL) ligand was prepared.► General formula of the synthesized complexes is [M(MPBT)$_2$]. ► Kinetic parameters (E_a, A, ΔH, ΔS and ΔG) have been calculated. ► Molecular modeling of the free ligand and its complexes has been calculated. ►Biological activities on different bacteria and fungal were examined.